Pacific Northwest
NATIONAL LABORATORY

PNNL-38975

Development of PNNL's Plutonium Metallography Capability

January 2026

Jacqueline Royer
Matthew Athon
Dallin Barton
Kayla Yano
Scott Swenson
Strother Cooper
Luke Sweet
Matthew Olszta
Dallas Reilly

U.S. DEPARTMENT of ENERGY

Prepared for the U.S. Department of Energy
under Contract DE-AC05-76RL01830

DISCLAIMER

PACIFIC NORTHWEST NATIONAL LABORATORY
operated by
BATTELLE
for the
UNITED STATES DEPARTMENT OF ENERGY
under Contract DE-AC05-76RL01830

Printed in the United States of America

Available to DOE and DOE contractors from
the Office of Scientific and Technical Information,
P.O. Box 62, Oak Ridge, TN 37831-0062
www.osti.gov
ph: (865) 576-8401
fox: (865) 576-5728
email: reports@osti.gov

Available to the public from the National Technical Information Service
5301 Shawnee Rd., Alexandria, VA 22312
ph: (800) 553-NTIS (6847)
or (703) 605-6000
email: info@ntis.gov
Online ordering: http://www.ntis.gov

Development of PNNL's Plutonium Metallography Capability

January 2026

Jacqueline Royer
Matthew Athon
Dallin Barton
Kayla Yano
Scott Swenson
Strother Cooper
Luke Sweet
Matthew Olszta
Dallas Reilly

Prepared for
the U.S. Department of Energy
under Contract DE-AC05-76RL01830

Pacific Northwest National Laboratory
Richland, Washington 99354

Summary

The goal of this project was to develop plutonium metallography capabilities and establish workflows for characterization at PNNL's Radiological Processing Facility (RPL). Developing and expanding on this capability opens more opportunities for PNNL to better support science through collaborations with other labs, plants, and sites withing the Department of Energy Complex and through programs within the National Nuclear Security Administration. This project established metallography equipment in an air glovebox, polishing protocols, as well as radiological and facility controls and procedures so that gram quantities of plutonium metal could be analyzed on multiple characterization tools. Data was collected and analyzed on two different delta phase plutonium - Gallium samples and a calciothermically reduced alpha plutonium metal using a combination of optical and electron microscopy, powder X-ray diffraction, and atom probe tomography. This report highlights the metallography capabilities, some preliminary data collections, and plans at PNNL to support plutonium material science.

Table 1. Equipment available for Pu metallography and characterization.

Equipment Type	Brand	Applicability
Metallographic Low Speed Saw	Buehler Isomet	Low speed saw used for subsampling bulk pieces of metal to target site-specific samples for metallography and characterization.
Autopolisher	Allied MetPrep 3	Removes scratches, oxide layers, and other surface defects for microscopy and other surface characterization techniques.
3D Optical Profilometer	Keyence VR-6000	Collects 3D surface data for measuring roughness, flatness, and sample profiles of material.
Digital Optical Microscope	Keyence VHX-7000	High-resolution imaging of materials and their surface microstructures.
Powder Diffractometer (XRD)	Rigaku Smart Lab	Measures X-rays scattered off a material. Provides information on crystal structure, phase ID, and lattice parameters grain size, orientation and defects.
Focused Ion Beam Scanning Electron Microscope (FIB SEM)	Thermo Fisher Helios Nanolab 660	Use of a gallium ion beam for precise material removal or deposition. Allows for small scale material preparation for APT, TEM, and site-specific cross sections.
Atom Probe Tomography (APT)	Cameca Local Electrode Atom Probe (LEAP) 5000 XR	Needle shaped samples subjected to high electric field, removing individual atoms from the surface which are then picked up by a detector. This provides 3D atomic scale imaging and chemical composition analysis.
Scanning/Transmission Electron Microscope (S/TEM)	JEOL GrandARM 300CF	Transmits electrons at high accelerating voltages through a thin sample. The resulting scattered electrons and interactions provide information on the materials' crystallography, chemical composition, and nanoscale structures.

Acknowledgments

This research was supported by the National Security Directorate Misson Seed Laboratory Directed Research and Development Program at PNNL. The work presented in this report was made possible by contributions from many people at PNNL's Radiochemical Processing Laboratory and through expert advice on metallography preparation from collaborators at Lawrence Livermore National Laboratory. Pacific Northwest National Laboratory is operated by Battelle for the U.S. Department of Energy (DOE) under Contract No. DE-AC05-76RL01830. Note: An AI-based language model was utilized to improve readability and ensure proper grammar and sentence structure for this report.

Acronyms and Abbreviations

APT	Atom Probe Tomography
BF	Bright Field
DOE	Department of Energy
EBSD	Electron Backscattered Diffraction
EDS	Energy Dispersive X-Ray Spectroscopy
FIB-SEM	Focused Ion Beam Scanning Electron Microscope
FY	Fiscal Year
HAADF	High Angle Annual Dark Field
LDRD	Laboratory Directed Research and Development
MgO	Magnesium Oxide
OM	Optical Microscope
PNNL	Pacific Northwest National Laboratory
Pu	Plutonium
α-Pu	Alpha Phase Plutonium
δ-Pu	Delta Phase Plutonium
RPL	Radiochemical Processing Laboratory
S/TEM	Scanning / Transmission Electron Microscope

Contents

Figures

Tables

1.0 Introduction

The metallographic preparation and characterization of plutonium (Pu) metal is a challenging operation due to its radiological hazards, chemical reactivity, and low oxidation resistance. Like uranium metal, freshly polished unalloyed Pu metal must be stored in an inert or evacuated environment, or it will readily oxidize or corrode due to air and moisture. Pu alloyed with gallium (i.e., meta-stabilized δ-Pu) exhibits an improvement in oxidation resistance over unalloyed Pu, but exposure to air for even a few seconds can prevent adequate characterization with many surface-sensitive techniques. Because of these challenges, careful metallographic preparation of Pu metal and transfer to desired characterization equipment requires knowledgeable staff and the appropriate equipment.

The analysis of Pu metal is essential to numerous programs within the Department of Energy (DOE) Complex. Historically, Pacific Northwest National Laboratory (PNNL) had limited capabilities and expertise in handling, polishing, and characterizing Pu metal. This restricted PNNL to collaborative projects in which the sponsor or collaborator provided Pu metal that has already been metallographically prepared for characterization. This created an opportunity to expand its expertise in Pu material science through an internal effort. By developing specialized Pu metallography techniques and applying advanced characterization methods, PNNL has worked to address the challenges posed by this complex and difficult material system.

This report details an internal Laboratory Directed Research and Development (LDRD) investment by PNNL to establish a metallography capability for Pu metal and to establish a workflow for preparing Pu metal surfaces for advanced characterization techniques. Additionally, it highlights preliminary data collected during the scope of this project during fiscal year (FY) 2023 through FY2024. The development of metallography techniques has continued since the completion of this effort, and the remainder of the characterization results will be released in subsequent publications.

2.0 Glovebox Metallography Setup

Defect free surfaces are critical for a variety of advanced characterization and surface science techniques on metal samples. It is common practice in metallurgical science to use a combination of grinding and polishing equipment with a systematic approach of applying coarse to fine grit polishing pads and/or particle suspensions to remove surface defects and reveal the underlying microstructure. Polishing Pu metal is especially challenging due to its inherent radiological and chemical hazards that it poses to workers handling it; therefore, it is standard practice that Pu metal be cut, ground, and polished within a radiological glove box. Prior to this project, no equipment or workflow specific for Pu metal polishing existed at PNNL's Radiochemical Processing Laboratory (RPL). Additionally, there were no inert atmosphere glove boxes available for equipment installation. It was known that RPL would be procuring and installing several inert-atmosphere glove boxes in future years, so this project utilized an existing air-atmosphere glove box that had space availability. All the work presented in this report was performed by cutting, grinding, and polishing Pu metal within an ambient air atmosphere. The goal was to perform most processing steps using non-aqueous lubricants and suspensions so that the workflow could be transitioned to an inert atmosphere glovebox in the future. This section details the equipment established for PNNL's Pu metallography capability at RPL. Specific polishing protocols and characterization workflows are discussed in Section 3.0.

The equipment in **Table 2** was procured, tested, and installed within the air glove box at RPL. When necessary, data transfer and/or service lines were routed though hermetically sealed passthrough connections. Some examples of the metallography equipment are shown in **Figure 1**.

Table 2. Equipment established for Pu metallography preparation capability.

Equipment Name	Purpose
Buehler Isomet Low Speed Saw	Metallographic saw for sectioning samples of interest.
Hauschild Speed Mixer	Epoxy mixer for producing bubble-free epoxy.
Allied HighTech MetPrep 3 Autopolisher	Commercial 3-sample autopolisher for grinding and polishing mounted samples.
Ultrasonic Cleaning Bath	Used for sample cleaning between polishing compounds and for final preparation steps.
Keyence VR-6000 Optical Profilometer	3D optical profilometer for high precision measurements of dimensions and surface finish.
Keyence VHX-7000N Digital Microscope	Digital microscope for microstructural imaging and metallography progress checks.

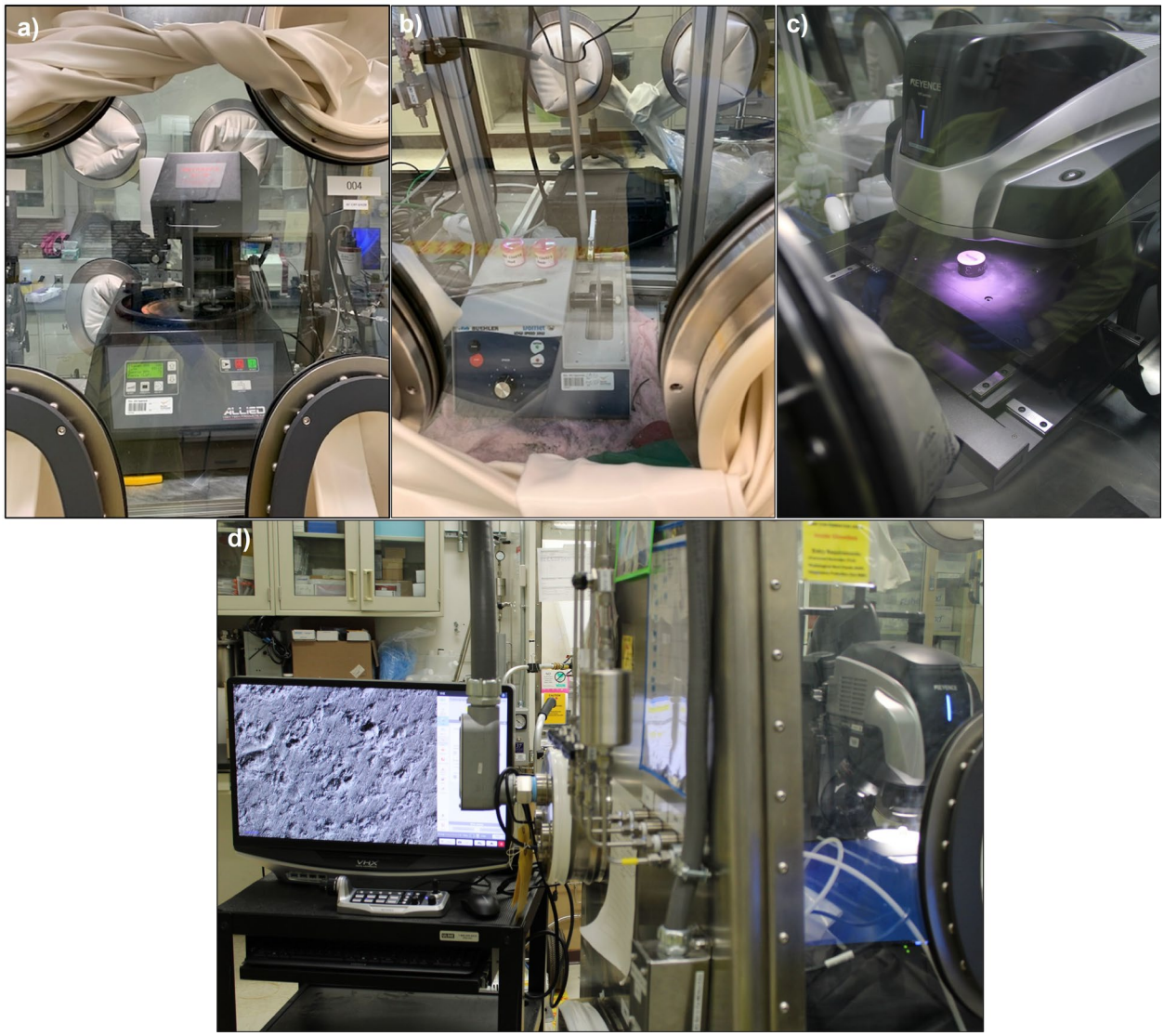

Figure 1. Example photos of metallography equipment installed in the air atmosphere glovebox including: a) variable speed auto polisher, b) metallographic low speed saw, c) 3D optical profilometer, and d) digital microscope with controls situated outside of the glovebox.

3.0 Sample Preparation and General Workflow

3.1 Background

Metallographic sample preparation typically follows these general steps: site-specific sampling, mounting in epoxy, grinding it into a planar surface, polishing to remove scratches and surface defects, cleaning the sample surface so that it is free from polishing compounds, and drying the sample [1]. This work followed this standard metallographic preparation, but it was tailored to Pu metal. Pu metal is highly reactive to water and oxygen, forming an oxide layer within seconds of exposure. Without access to an inert atmosphere glovebox, all polishing protocols required non-aqueous lubricants and rapid movement of finely polished samples from the glovebox to the characterization equipment.

The samples studied here were two different specimens including a Pu-Ga delta phase alloy (δ-Pu) and one calciothermically reduced alpha phase Pu (α-Pu) metal produced at PNNL (**Table 3**). The δ-Pu sample was produced at a partner laboratory but is considered scrap material. The purpose of sampling two types of Pu metal was to build a workflow and understand the polishing behavior of unalloyed Pu and a common Pu alloy. These two materials exhibit different mechanical behaviors due to their different crystal structures, and thus the approach for their final polishes varies. For example, it is well known that the face centered cubic (FCC) δ-Pu is softer and more ductile than the brittle monoclinic α-Pu, so this requires users to lower the polishing pressure of the auto polisher and to use less abrasive polishing compound (e.g., aluminum oxide) during final polishing stages on δ-Pu. **Figure 2** displays the general workflow PNNL used for polishing Pu metal in this study. This workflow was tailored based on the sample starting condition and the final desired surface finish. The specific details of PNNL's metallography procedure can be obtained by contacting the corresponding author of this report.

Table 3. Details of plutonium samples characterized for this study.

Sample Name	Description
δ-Pu	Pu alloyed with Ga
α-Pu	Unalloyed, produced by calciothermic bomb reduction

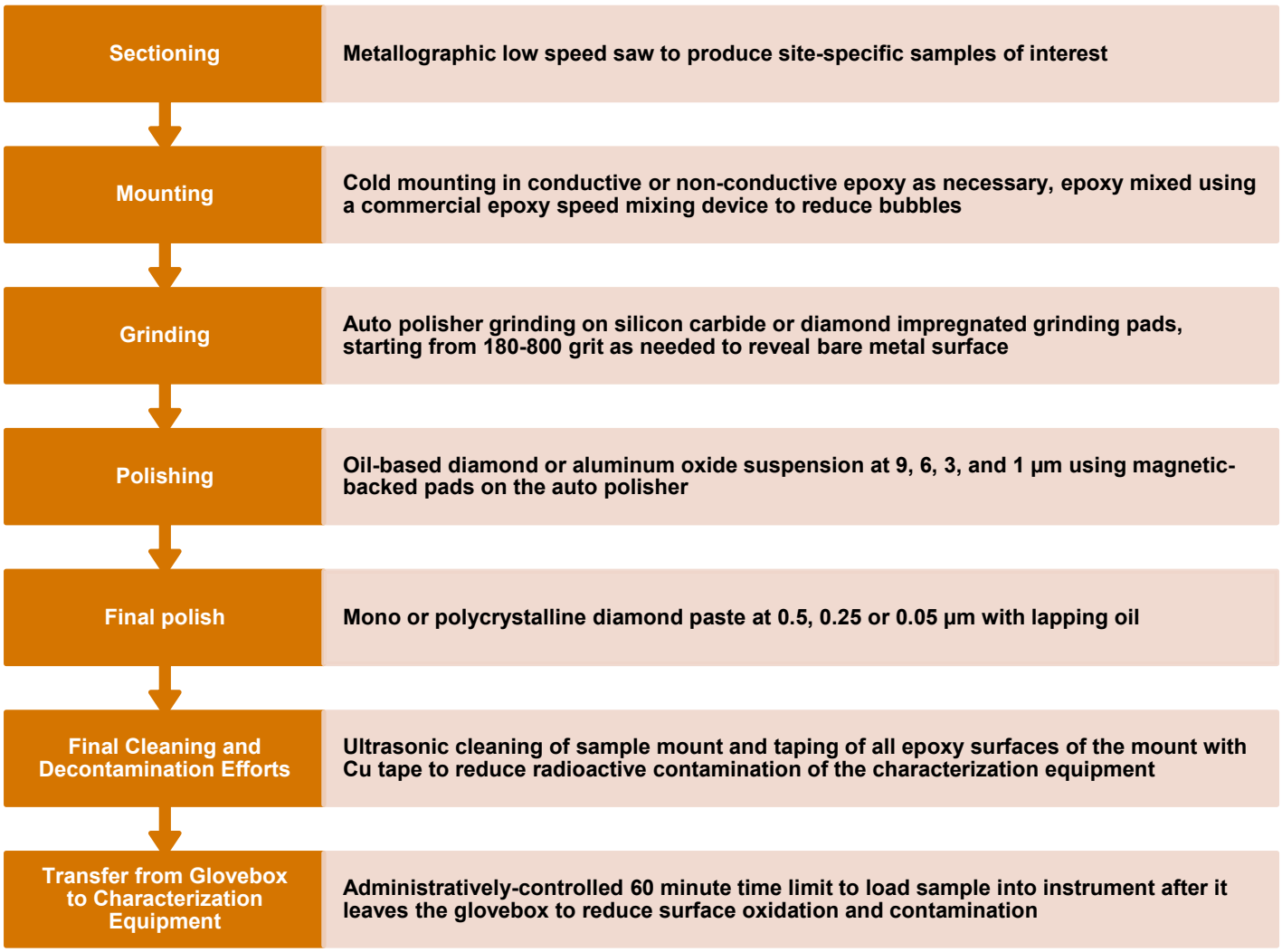

Figure 2. Overall Pu Metal Analysis Workflow.

The Pu samples in this study were both cast in two-part epoxy doped with conductive nickel filler to help prevent charging on the focused ion beam scanning electron microscope (FIB-SEM). Example images of these samples contained in epoxy and polished using the auto polisher are shown in **Figure 3**.

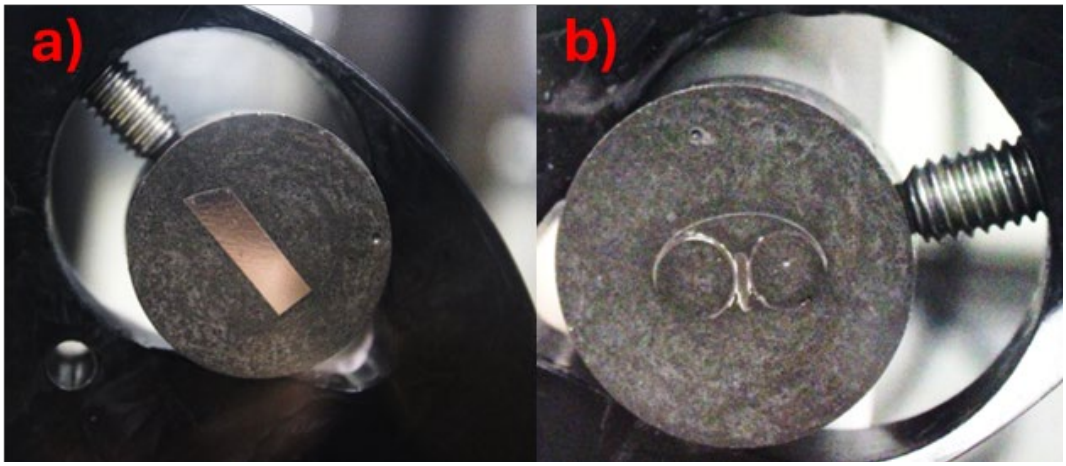

Figure 3. Mounted plutonium metal samples including a) α-Pu metal in a conductive epoxy mount and b) δ-Pu (center of mount) in a conductive epoxy mount secured in a mounting clip.

3.2 Challenges and Lessons Learned

Despite critical improvements in Pu polishing workflows and capabilities made possible by this project, there are still challenges to overcome. For example, achieving a fully scratch-free sample surface with the current mechanical polishing setup remains a challenge. During most of the process development, the digital optical microscope was not installed in the glovebox which limited the staff's ability to track the progress of the polishing. The optical profilometer was useful for determining sample flatness, but it lacked the optical resolution needed to see the sample's microstructure. It is expected that PNNL will continue to develop improved mechanical polishing methods using the digital microscope in FY26. Additionally, oxidation and the stringent radiological and contamination controls further complicated sample preparation and analysis workflows, adding additional layers of complexity to handling and preparing materials. It is expected that moving these capabilities into an inert glove box will help mitigate the challenges of surface oxidation experienced during the FY23-24 campaign.

An initial goal for this work was to use a newly installed Thermo Fisher Helios 5 UX FIB-SEM equipped with Oxford energy-dispersive X-ray spectroscopy (EDS) and electron backscatter diffraction (EBSD) detector. However, delays in the installation of this equipment in RPL necessitated the use of the existing Thermo Fisher Helios Nanolab 660 FIB-SEM. Unfortunately, the EDS and EBSD systems on the Nanolab 660 faced ongoing issues prior to their scheduled replacement in late FY2024, which resulted in limited EDS data being collected during these campaigns. It is expected that PNNL will perform more EDS analysis on these samples in FY26 using the new detector. EBSD analysis was not pursued due to the lack of inert transfer capabilities and Pu's rapid oxidation rate. Further method development on vibratory polishing, electropolishing, ion polishing, and rapid inert transfer for producing EBSD-quality finishes on Pu is required.

4.0 Characterization Results and Discussion

The main goal of this effort was to establish a workflow for metallographically preparing Pu metal for performing advanced characterization techniques. The following sections briefly document the employed techniques and the initial observations of the microstructure at increasing resolution and detail. The data presented here is considered preliminary and will be released in full in future publications.

4.1 Optical Microscopy

Establishing optical microscopy (OM) and profilometry capabilities is crucial for developing an effective metallography workflow for Pu metal. These tools enable the evaluation of scratch sizes, ensuring surface damage from earlier polishing steps is progressively minimized. Additionally, they provide valuable insights into microstructural features and grain size, supporting precise and reliable sample preparation.

A Keyence VHX-7000 digital optical microscope and a Keyence VR-6000 optical profilometer were used during polishing to assess the material surface throughout polishing. **Figure 4** shows images using the VR-6000 Profilometer on α-Pu and δ-Pu after 1 and 3 μm polish suspensions. Digital optical microscopy images at various stages of polishing progression of δ-Pu using the digital microscope can be seen in **Figure 5**.

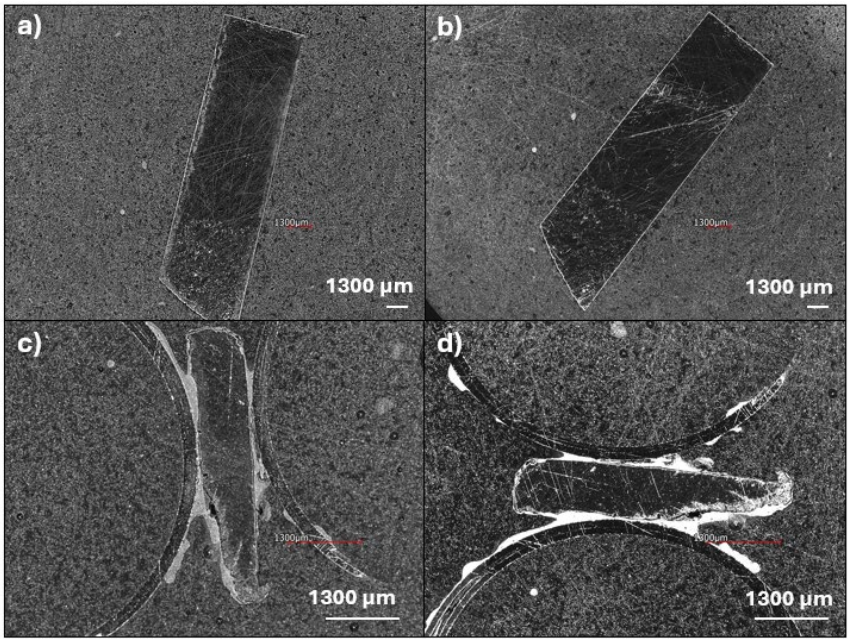

Figure 4. VR-6000 Profilometer Images of α-Pu a, b) and δ-Pu-2 c, d) after 3 a, c) and 1 μm b, d) polishing suspensions.

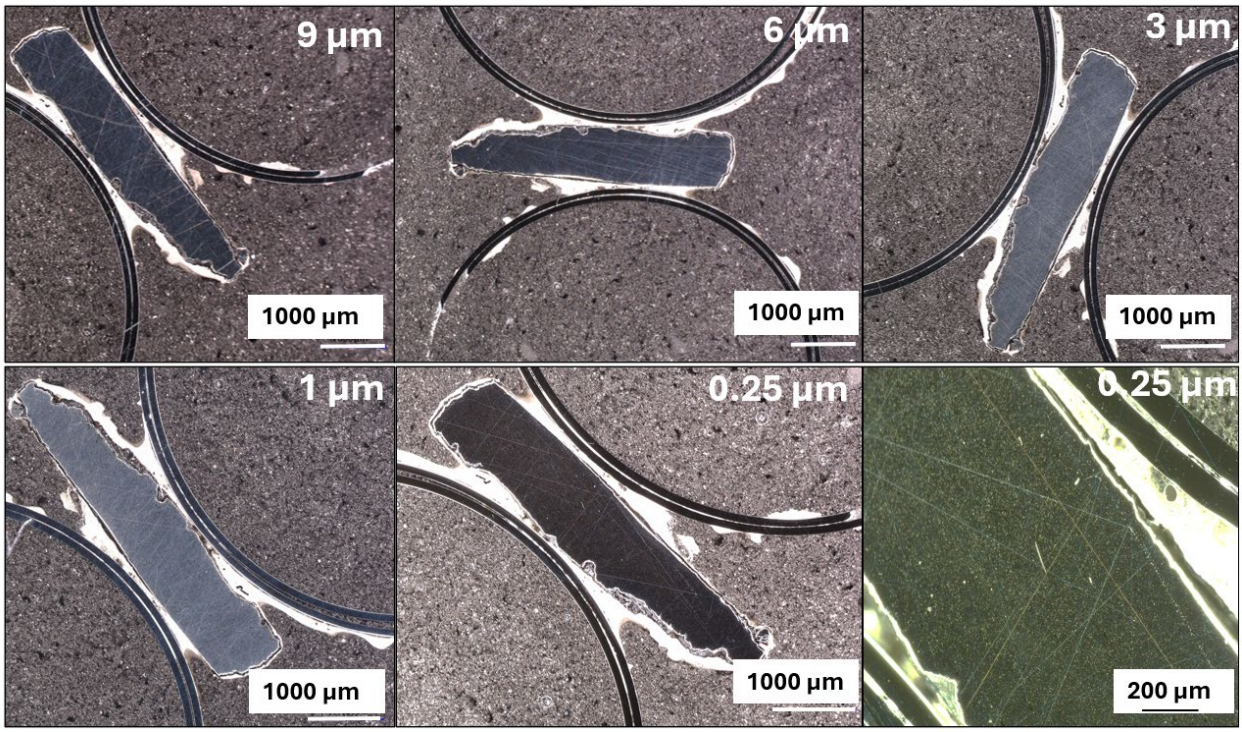

Figure 5. Keyence VHX-7000 digital optical microscope showing the progression of δ-Pu sample after 9, 6, 3, 1, and 0.25 µm diamond suspensions.

4.2 Scanning Electron Microscopy

Scanning electron microscopy provides higher resolution imaging of the samples surface as well as capturing composition-sensitive information through EDS and backscatter detectors. Two examples of features observed with SEM are provided here.

Figure 6 displays a secondary electron image with corresponding EDS maps of a common inclusion in the α-Pu sample, which was produced through calciothermic bomb reduction. This sample underwent final polishing using a non-aqueous colloidal silica polishing suspension, which caused substantial etching of the metal surface within seconds of exposure. This suspension was not tested further or utilized in subsequent Pu preparations due to chemical reactivity concerns. The multi-phase inclusion shown in this EDS map included a ring of nitrogen and Pu, which is assumed to be a nitride species. Within the core of that inclusion was a magnesium and oxygen rich region which is likely magnesium oxide (MgO). During the bomb reduction process, PuF_4, calcium, and iodine are mixed and loaded inside of a MgO crucible. The reaction vessel and reagents undergo a rapid thermal reaction (>1500°C) as the calcium reduces the PuF_4 to Pu metal. The authors interpret this inclusion as an artifact of the bomb reduction, which is possibly a signature of how it was produced.

Figure 7 displays lower magnification concentric backscattered (CBS) detector images of the α-Pu and δ-Pu samples. There is a much higher volume fraction of globular and faceted secondary phase inclusions in the α-Pu, which is expected due to the low solid solubility for impurities in this crystal structure. The α-Pu here is in the as-bomb reduced state, meaning that it has not been purified of process contaminants. Morphological analysis using image

segmentation or machine learning was outside of the scope of this project; however, Pu materials science would benefit from quantitative morphological characterization of the inclusions in these types of samples.

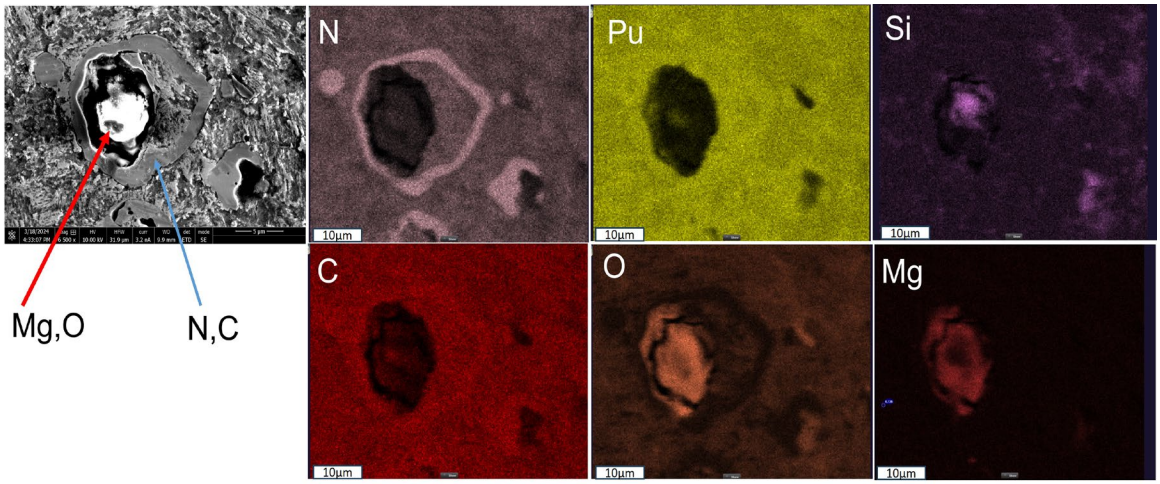

Figure 6. α-Pu metal EDS scan of a secondary phase inclusion revealing the presence of nitrogen, silicon, oxygen, and magnesium.

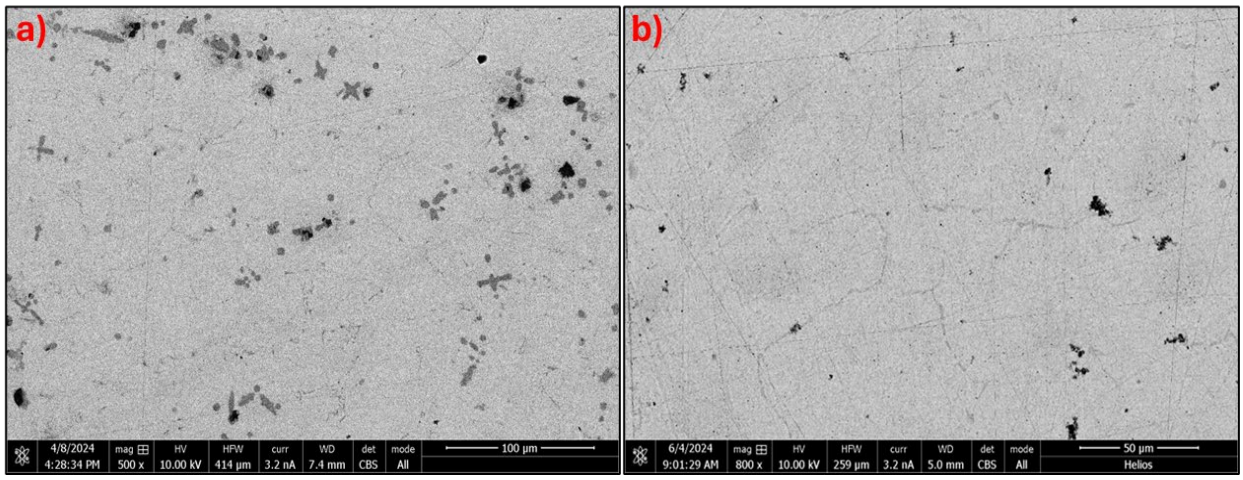

Figure 7. Concentric Backscatter Detector (CBS) image of α-Pu a) sample at 500x and δ-Pu b) sample taken at 800x magnification.

4.3 Focused Ion Beam Sample Preparation

A Thermo Fisher Helios Nanolab 660 Ga FIB-SEM was used to prepare all S/TEM and Atom Probe Tomography (APT) specimens analyzed in this report. For S/TEM samples, a standard procedure for FIB preparation was used by first focusing on the sample, identifying the eucentric height, and selecting the region of interest. A protective layer of Platinum (Pt) and/or carbon (C) was deposited using the electron beam and then ion beam at 0° and 52° tilt, respectively. Trenches were milled on either side of the lamella, followed by cleaning and undercutting to isolate the region. The lamella was extracted via micromanipulator, brazed to a S/TEM grid using Pt and/or C, and detached from the manipulator. Gradual thinning was performed by

milling windows on both sides of the lamella while progressively adjusting the tilt angle and gradually reducing voltage and current settings while monitoring its thickness until electron transparency was achieved (~100-300 nm). Final polishing was done briefly at low beam energies (2 kV) to minimize damage. **Figure 8** presents a series of SEM images depicting a few of the key stages of TEM sample preparation via FIB on an α-Pu inclusion: selection of the area of interest, trenching to isolate the lamella, initial thinning to approximately 400 nm, and final thinning to achieve electron transparency. These general steps were modified as necessary, depending on the sample behavior and the judgment of the FIB operator.

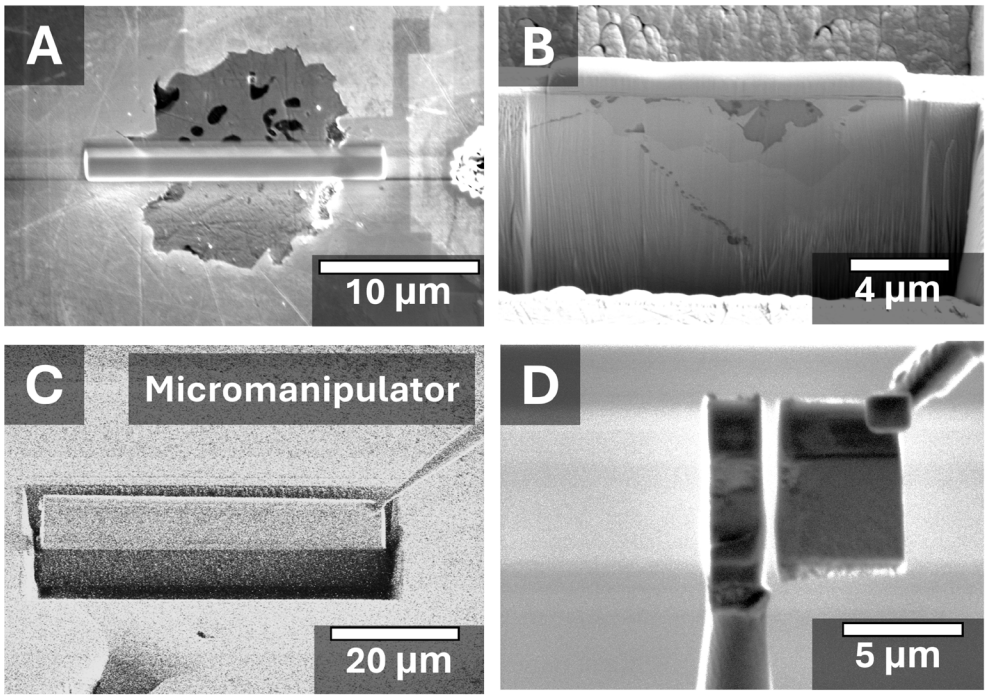

Figure 8. Secondary electron image series of the “liftout” method for APT and TEM sample preparation on an α-Pu sample using FIB-SEM including; a) protective Pt or C cap on top of a region of interest, b) milling trenches to the sides of the protective cap to isolate the lamella, c) undercuting the sample, and brazing to a micromanipulator. d) Brazing a sample from the micromanipulator onto a coupon for final sample preparation.

Pu metal proved challenging to thin for TEM due to its susceptibility to FIB-induced hydriding/ beam damage, re-sputtering, and curtaining effects (see **Figure 9** and **Figure 10**). When preparing lamella containing inclusions, differences in material hardness and composition across the sample led to uneven milling rates. While this study did not primarily focus on optimizing Pu FIB preparation for TEM, ongoing efforts at PNNL aim to improve lamella preparation through cryogenic techniques and fine-tuning thinning parameters.

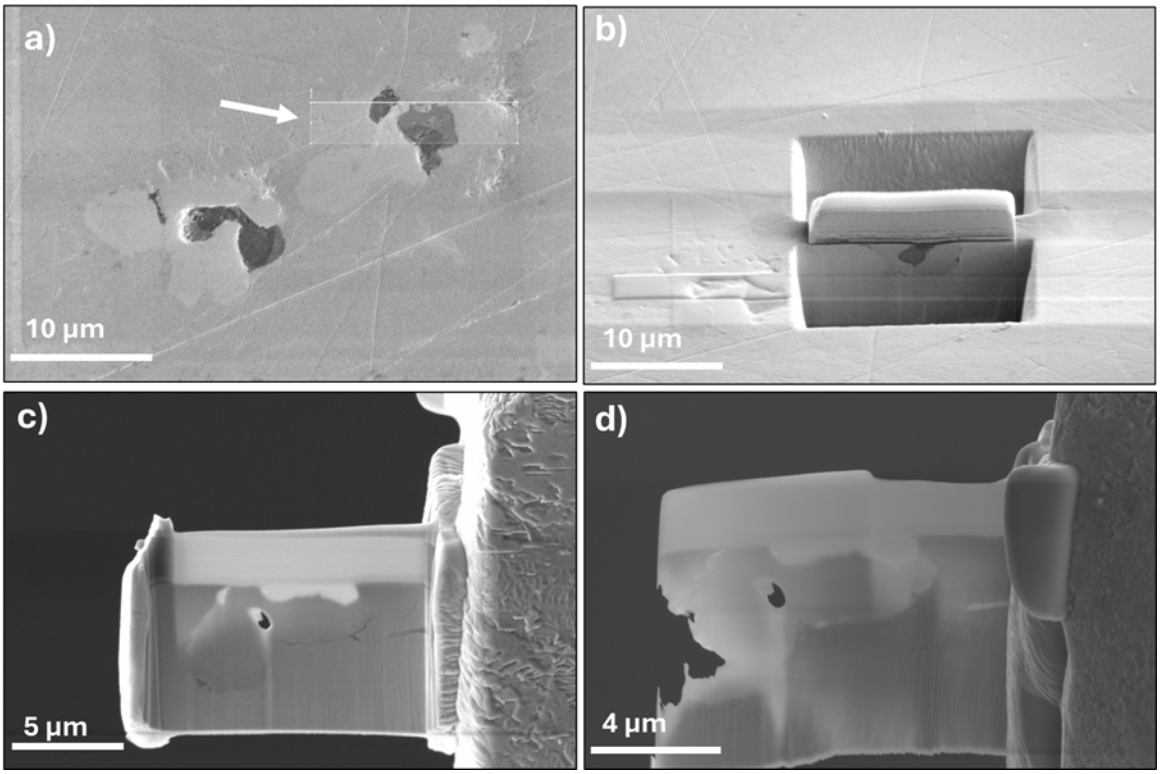

Figure 9. TEM lamella preparation progression from α-Pu where an area of interest at an inclusion was selected, a) lifted out , b) and thinned to electron transparency (c and d). TEM analysis of this inclusion is discussed in section 4.4.1.

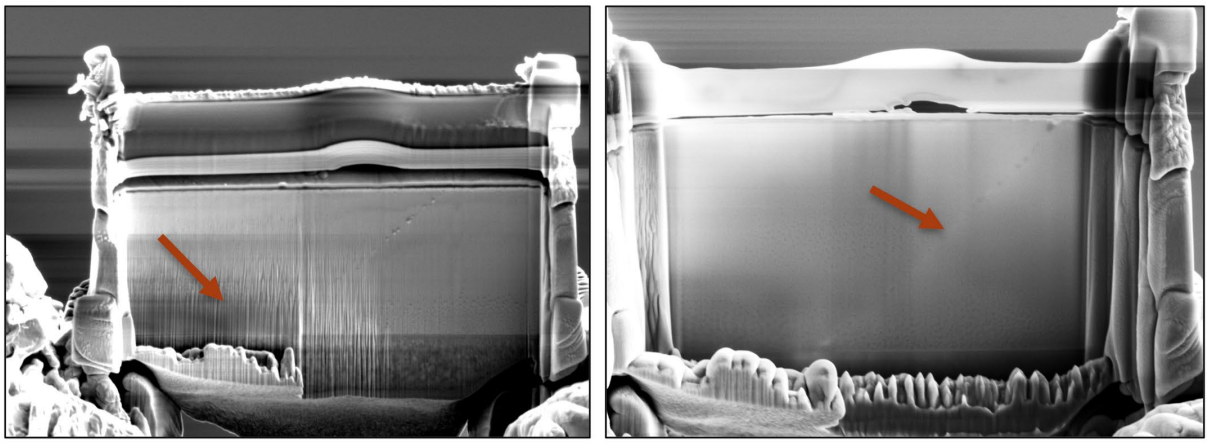

Figure 10. δ-Pu liftout during thinning procedures, red arrows showing curtaining (left) and the formation of hydrides along the grain boundary (right).

APT samples were made via the “liftout” method using a FIB-SEM like the TEM sample preparation process. The bulk sample was cross-sectioned using a FIB-SEM and undercut at a specific region of interest. The undercut portion is then brazed to a micromanipulator needle, lifted out of the bulk sample and then brazed to a silicon coupon with posts that are pre-sharpened to a 1 µm diameter, **Figure 11**. The samples are then sharpened using the FIB-SEM to a final needle-like shape with the diameter of < 100 nm.

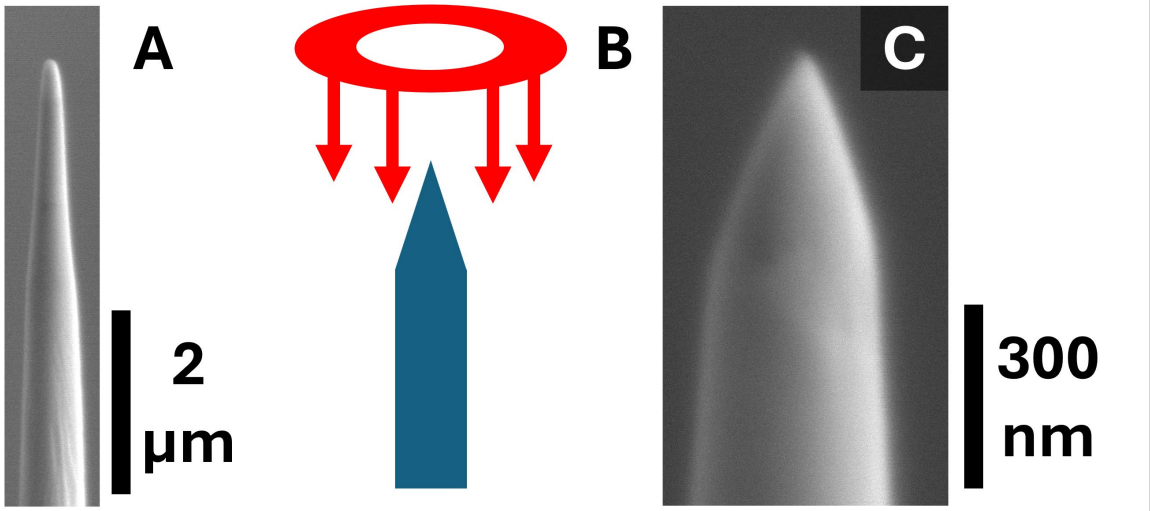

Figure 11: Final preparation of APT samples. a) Secondary electron image of an APT sample tip ready to be final thinned. b) Cartoon of the annular FIB milling on top of the tip. c) Image of the final thinned tip.

4.4 Scanning / Transmission Electron Microscopy

S/TEM was used to analyze inclusions, phase chemistry, and crystallography in both Pu-Ga alloys and bomb reduced α-Pu metal. The addition of S/TEM into the characterization workflow of Pu is important due to its ability to study materials down to the atomic scale at high resolution (<0.1 nm). This allows one to better understand the material's crystallographic and chemical information at the nanoscale, enabling characterization of phenomena such as elemental segregation at grain boundaries, dislocation type and density, phase precipitation, and changes to lattice parameters in localized regions.

The S/TEM studies of the α-Pu sample primarily focused on analyzing inclusions and identifying potential impurities introduced during the bomb reduction process. In contrast, the S/TEM analysis of δ-Pu sample was aimed at investigating the extent of the mechanically induced phase transformation from FCC δ-Pu to monoclinic α'-Pu in addition to any inclusions or impurities. The data presented here is representative of the approach developed during this LDRD and is not exhaustive. It will be fully released in future publications.

4.4.1 Alpha Pu Inclusion Analysis

S/TEM was employed to analyze the inclusions in bomb-reduced α-Pu, revealing complex inclusions consisting of Mg, Ni, Cr, C, N, and O. An SEM CBS detector image of the inclusion is showcased in **Figure 12**. This region is then lifted out and the cross-section is captured with bright field (BF) and high angle annular dark field (HAADF) detectors (**Figure 13**). HAADF image contrast is based on atomic number differences (Z-contrast) while BF imaging is primarily phase contrast. Paired with EDS maps, (**Figure 14**) the imaging and compositional characterization highlights a distinct darker Mg-rich inclusion, abutting a lighter N-rich inclusion, both outlined with an irregular Ni-rich "shell". The presence of Mg in the S/TEM data, as

highlighted in **Figure 14**, is understood to be an artifact of the bomb reduction process, as previously discussed in Section 4.2. Further investigation is required to fully understand the presence and formation mechanisms of these inclusions within bomb reduced α-Pu.

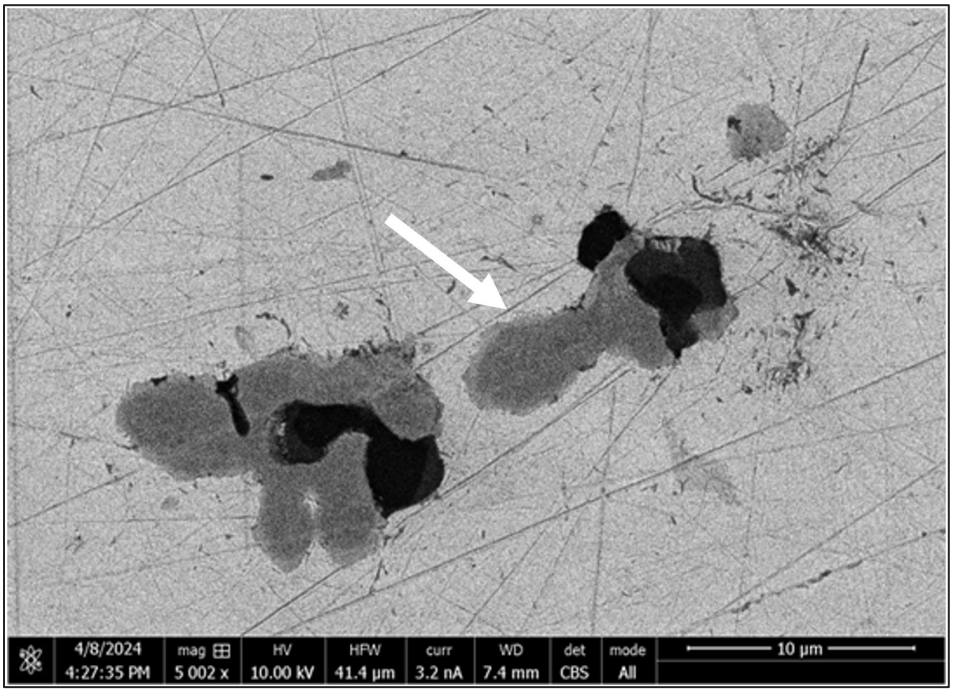

Figure 12. SEM image of a Mg-bearing inclusion (white arrow) in α-Pu that was prepared for S/TEM analysis.

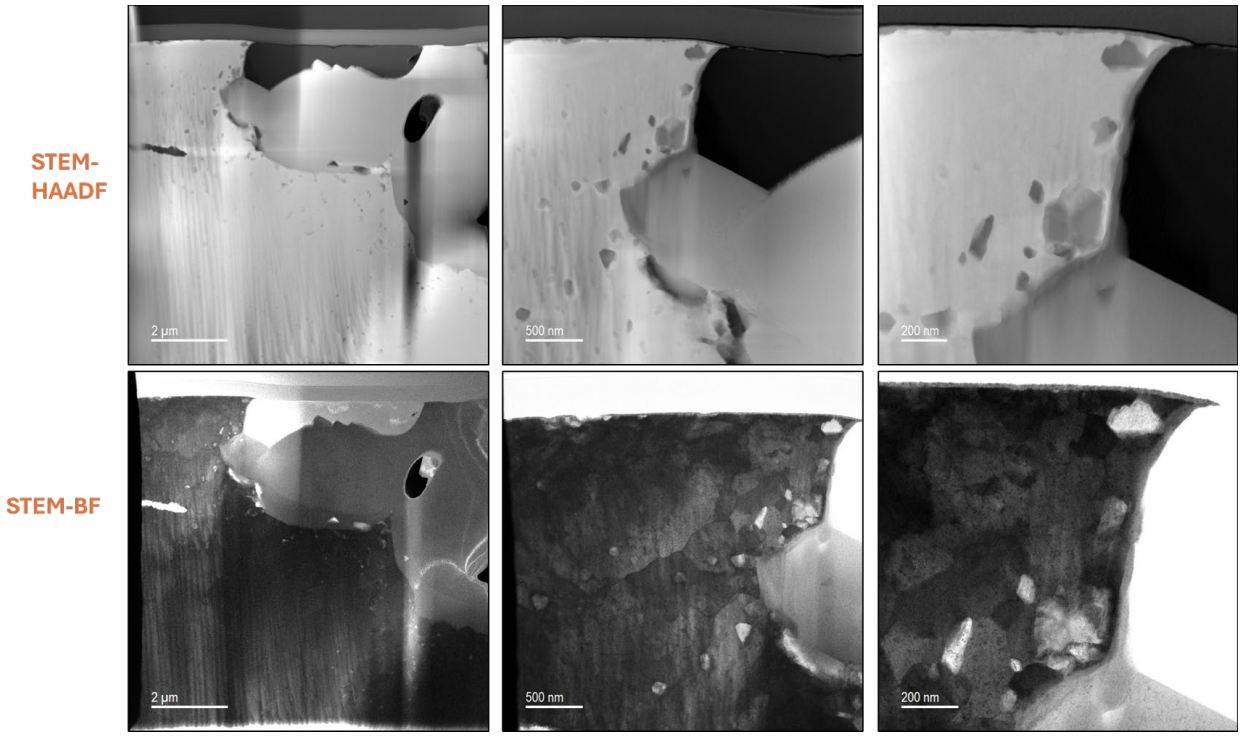

Figure 13. S/TEM HAADF images (top) and BF images (bottom) of inclusions within the α-Pu.

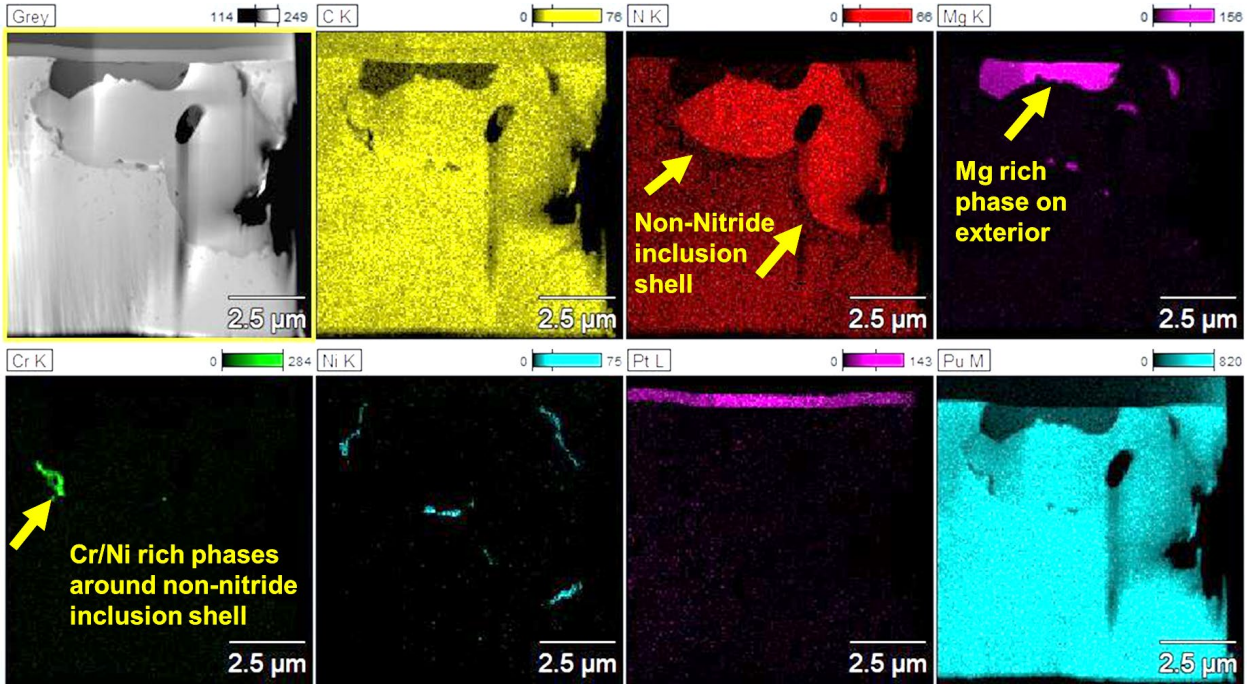

Figure 14. S/TEM EDS of α-Pu inclusions revealing the presence of complex Mg and N rich inclusions surrounded by irregular Ni and Ni/Cr rich shells.

4.4.2 Delta Pu Damage Layer and Inclusion Analysis

Gallium (Ga)-stabilized δ-Pu is subject to strain-induced martensitic phase transformation. Currently, there are limited reports and data on this effect as a product of metallographic preparation. The two phases have significantly different properties. The monoclinic α'-Pu has a higher density, typically around 19.86 g/cm³, compared to the δ-phase, which has a density of approximately 15.8 g/cm³ [2]. In addition, α'-Pu exhibits increased hardness compared to δ-Pu. These differences in density and hardness significantly impact the handling, machining, and mechanical stability of Pu components. Understanding this phase change is critical for optimizing processes such as sample preparation and predicting material performance in various applications. A previous study of this phase transformation reported a 7.6 µm deep damage layer after mechanically polishing to 1 µm diamond paste and were able to fully remove this layer through electropolishing [3]. S/TEM analysis of the δ-Pu sample was used to study the extent of phase transformation that occurred because of mechanical polishing procedures used in this work.

δ-Pu was final polished using a 0.05 µm diamond paste and 45 lbf pressure central force holder. Standard metallographic and cleaning protocols were employed as described in Section 3.0 of this report. Two TEM samples were generated from the bulk material using the FIB-SEM and transferred to the TEM via rapid air transfer. The two TEM samples analyzed include one liftout containing a grain boundary and another representing the bulk metal. HAADF images show the depth of the α' layer in **Figure 15**. Here, elements with higher atomic numbers (Z) and/or a higher-density phase scatter electrons more strongly, thus appearing brighter in HAADF images, while lower Z elements or lower-density phases appear darker. In each of the HAADF images (**Figure 15a & d**), distinct layers are visible: the darker contrast platinum capping at the top, followed by the oxide layer, the lighter contrast α' layer, and the bulk FCC δ-Pu material below. Within the bulk material, darker hydrides are distributed throughout the sample, primarily a result of FIB artifacts [4] and will not be further discussed in this report. The α' layer in the bulk material (**Figure 15d**) was approximately 70 nm thick, while near the grain boundary (**Figure 15a**), the damaged layer was between 100-150 nm thick. This 70-150 nm α' layer is significantly thinner than the 7.6 µm deep α' layer reported in Pu-3.3 at.% Ga by Wallace et al., 1988 [3], characterized using XRD and profilometry after final polishing with 1 µm diamond paste.

Selected Area Electron Diffraction (SAED) was collected in the region identified by the white circle in **Figure 15a** to confirm the presence of the δ-phase (**Figure 15e & f**). The α' damaged layer was nanocrystalline and SAED ring patterns suggest a mixture of oxide and α' present.

Additionally, STEM EDS maps were taken of the liftout at the grain boundary and maps for the Pu M and O K edges are provided in **Figure 15b & 15c**. Here, we can see what looks to be darker potential “inclusions” along the grain boundary and throughout the material. EDS helped to confirm that these were likely Pu hydrides resulting from hydrogen uptake during FIB milling, as they had a slight depletion in Pu, though no other elements were detected. Their darker color also indicates a weaker Pu signal and lower density material compared to the surrounding δ-phase and very bright α’-layer. Additionally, the oxide layer identified by the stronger O signal is confined to the surface, suggesting limited oxidation depth into the sample.

The number of campaigns conducted for this study was constrained by several factors, including limited instrument availability, budget restrictions, glovebox access, and radiological controls that limited sample handling time. Consequently, only one TEM campaign on **δ-Pu** was performed with a 0.05 µm diamond paste as the final polish. Future work will assess and

compare the extent and depth of the α' damage layer using various final polishing abrasion particle sizes.

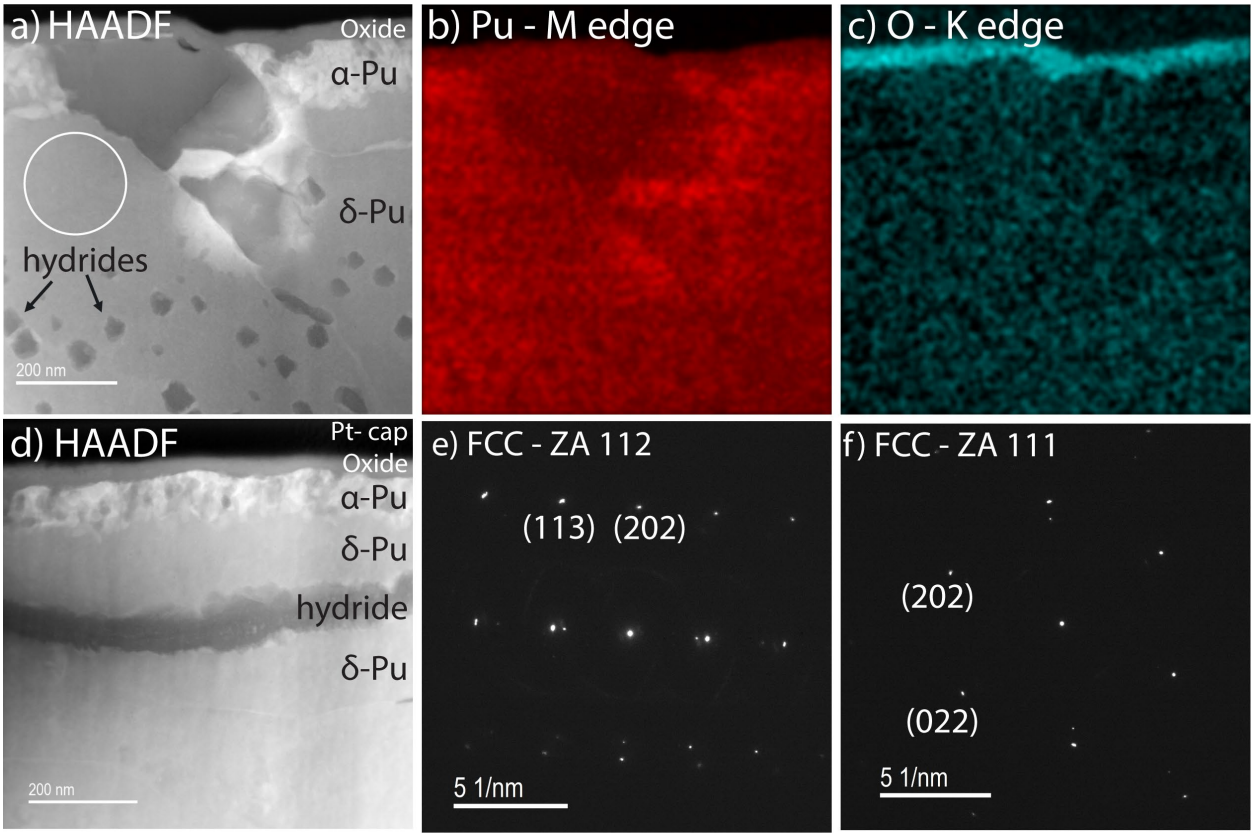

Figure 15. S/TEM HAADF image from two different FIB liftout locations of δ-Pu that was polished down to 0.05 μm. Liftout a) taken from grain boundary with α' damage layer varying between 100-150 nm thick. Accompanying EDS maps b, c) confirm slight depletion of Pu in hydrided regions and oxygen present at the surface layer. Liftout d) taken from the bulk material with α' damage layer approximately 70 nm thick. SAED images e) and f) from circled region in a) confirm FCC δ-phase in the matrix.

4.5 X-ray Diffraction

X-ray diffraction (XRD) was performed on a Rigaku Smart Lab powder diffractometer to further investigate the extent of the α' damage layer in δ-Pu polished to 0.5μm diamond paste. δ-Pu, α-Pu, and PuO_2 peaks were observed at a 74 nm probe depth (**Figure 16**). This XRD data corroborates observations of an α' damage layer at 70-150 nm deep observed in the TEM analysis. The observations of a Ni metal peak are due to the presence of conductive filler in the epoxy.

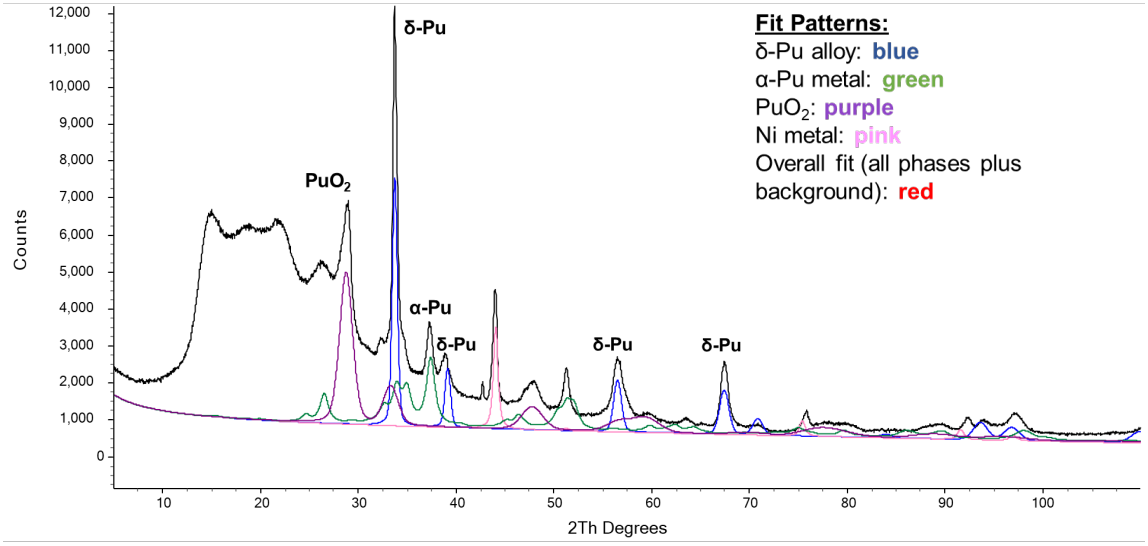

Figure 16. XRD of 0.5 um polished δ-Pu sample showing an alpha phase peak at 74nm probe depth.

4.6 Atom Probe Tomography

APT is a technique that produces a 3-dimensional data map of materials. Optimized data collection and analysis can produce data with sub-nanometer resolution and close to parts per million chemical sensitivity. The sample is subjected to a kilovolt electric potential and laser pulse that produces an energy density > 1E12 V/m. The field density allows an atom to ionize and evaporate off the surface and strike a position-sensitive detector. The pulsing energy and detector provide time of flight information that can be converted to a mass spectrum. The chemical information from the mass spectrum is then combined with the position information from the position-sensitive detector and the needle-shaped sample is reconstructed into a 3-dimensional chemical-position map where every data point is nominally an ion. From this dataset, compositional trends about the sample can be interpreted.

Preliminary APT data from δ-Pu is shown in **Figure 17**. Pu readily oxidizes in air. The current transfer method involves venting the FIB-SEM vacuum chamber and transferring into the APT LEAP vacuum chamber which leads to the tips exposed to atmosphere. Because of that, it was difficult to obtain pure Pu metal data.

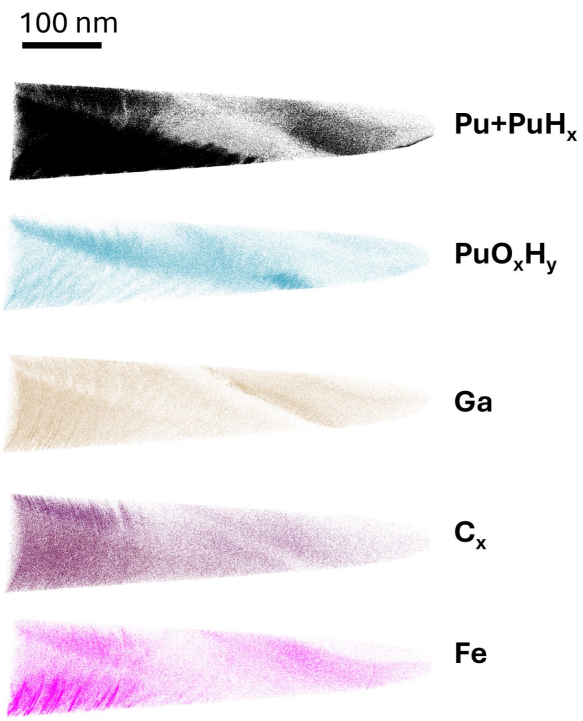

Figure 17. δ-Pu APT 3-dimensional volume rendering showing heterogeneous segregation of $Pu+PuH_x$ (black), PuO_xH_y (light blue), Ga (brown), C (magenta), and Fe (pink).

The Pu and Pu oxides appear to be lathes instead of purely homogenous. Additionally, trace amounts of Fe were present in the material. An Fe-rich region is seen around a depleted Pu region and is present with additional Ga and C. The singular straight line indicates that it is likely on a grain boundary. This work was performed when the EDS detector on the FIB-SEM was not operational, which limited the micron-scale chemical characterization of the inclusions. As of FY25, EDS detectors are available for targeted analysis of inclusions and interfaces in Pu metal samples.

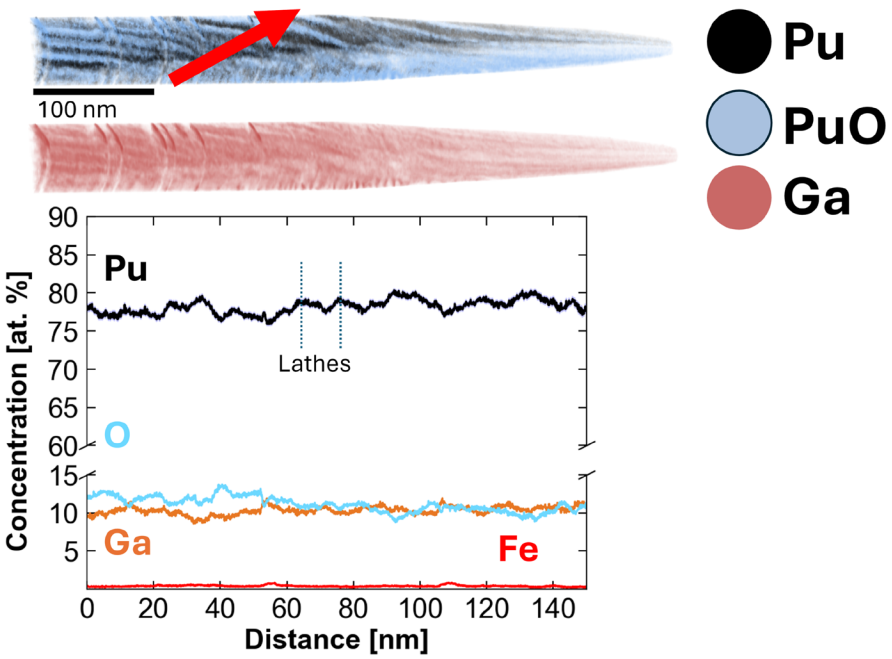

Figure 18. Ion maps of δ-Pu. These maps are binned and represented via 3-D volume rendering with Pu as black, Pu oxide as blue and Ga as red-brown. A 1-dimensional concentration profile taken across the red is represented showing decomposed Pu, O, Ga, and Fe.

Figure 18 shows a 1-dimensional concentration profile shows the concentration differences within the specimen. Pu and oxygen concentrations vary about 5 at. %. There are also trace amounts of Fe found that is not heterogeneously distributed throughout the material.

A targeted APT analysis of the Mg bearing inclusions in the α-Pu sample was attempted. A section of this material was identified using contrast differences using SEM and then target milled into APT samples, **Figure 19**. This FIB-milled cross section cut shows several different contrasts. The first contrast on top is over contrasted so that we can view the cross section easier. The second layer is Pt that is deposited to protect the samples from ion beam damage. In the cross-section, there are three major contrasts: the darkest in the core, the middle darkness surrounds the core, and then the lightest appears to be the base metal. These different contrasts were targeted during different sharpening processes.

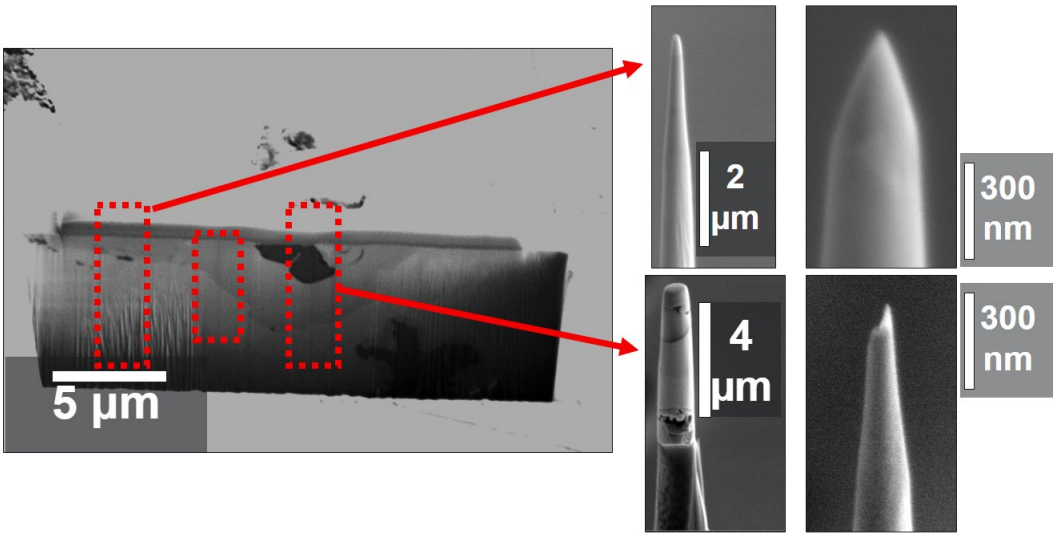

Figure 19. FIB-milled cross section of α-Pu cut revealing the inclusions in the Pu metal and then a couple of the final atom probe samples created.

The first APT data collected for the α-Pu was in a region with elevated Mg and N, **Figure 20**. Ion maps show a sampled location of the ions within the data. From visual inspection, there are no defects or spatial heterogeneity of the constituent elements.

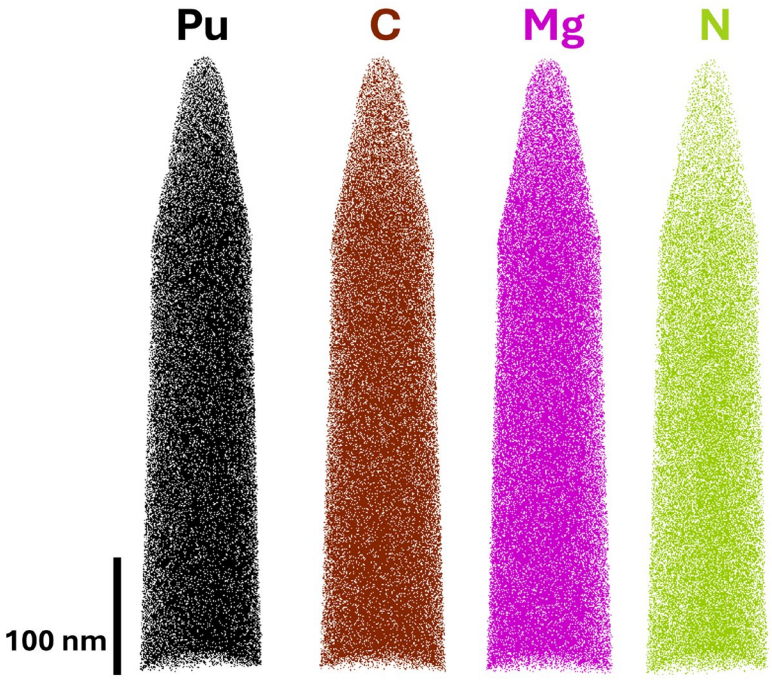

Figure 20. Ion maps of the Pu-Mg-C with trace N.

Total elemental composition of the tip is given in **Table 4**. The tip is Pu mixed with Mg and C with small amounts of N and Al.

Table 4. Measured composition of the entire sample of the Pu-C-Mg-N in Figure 21.

Element	Concentration (at. %)
Pu	76.14
C	15.14
Mg	8.60
N	0.07
O	0.05
Al	0.003

APT data was collected across the interfaces of other inclusions in the α-Pu. **Figure 21** shows a N-rich region and a C-rich region. The red dotted arrow (**Figure 21a**) represents the area in which a 1-dimensional concentration profile of the data is measured and graphed in **Figure 21c**. The process of collecting APT data involves pulsing energy onto a tip of the sample resulting in a field evaporation event evaporating one atom at a time. This pulsing energy results in constant pressure across the entire sample which eventually causes a catastrophic fracture of the sample. This sample fractured before achieving a steady-state concentration in the C-rich region. Nevertheless, there is some interesting behavior in this specimen. First, Ca was present throughout the sample, presumably present from the calcium reductant used in the bomb reduction process. Ca is present slightly more in the N-rich phase than the C-rich phase. Ti and F impurities were found in the C-rich phase that is not present in the N-rich phase. There is also a ~ 5 at. % O that increases in the C-rich phase. The increased presence of O in the C-rich phase may look a little surprising as C reduces oxides, but the concentration profile is still showing a transitioning area. In this location, it may be energetically favorable for O to segregate in this interface rather than in the matrix of either phase.

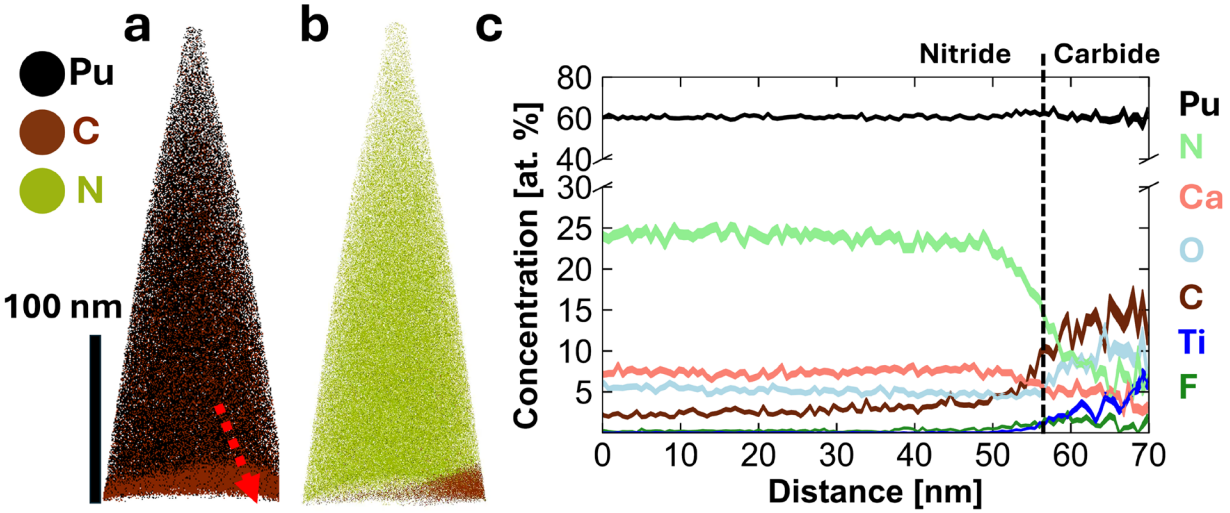

Figure 21. APT of Pu-nitride and Pu-carbide and the interface. a) Ion map of Pu (black) and C (brown). b) Ion map of Pu (black) and C (brown). c) 1-Dimensional concentration profile across the arrow shown in the ion map transitioning across the interface from the N-rich region to the C-rich region.

An interface between a Mg-rich region and a Pu-N-rich region, **Figure 22**, was captured. **Figure 22a** is an ion map showing the different ion species with Mg (pink), C (brown), N (green), and Pu (black). The red dotted arrow on the ion map shows where the 1-dimensional concentration

profile is measured and is graphed in **Figure 22b**. A higher-magnification portion of the interface of the concentration profile is graphed in **Figure 22c**. The Mg-rich region has small amounts of O and Ca. This interface is unexpectedly wide where the concentrations of N increase from ~0 at. % up to about 25 at. % N concentrations. At maximum concentrations of measured N, there are few impurities outside of N and Ca. However, the interface shows some interesting behavior. Within the interface between the Mg-rich region and the N-rich region, there are peaks of two different contaminants. Closer to the Mg-rich region, there is an increase in Cu concentrations from ~ 0 at.% to ~ 3 at. %. Total elevated Cu concentrations are about 40 nm wide. In between the Cu elevated concentration and the N-rich region, there is a peak in C concentrations from ~1 at. % to 10 at. %.

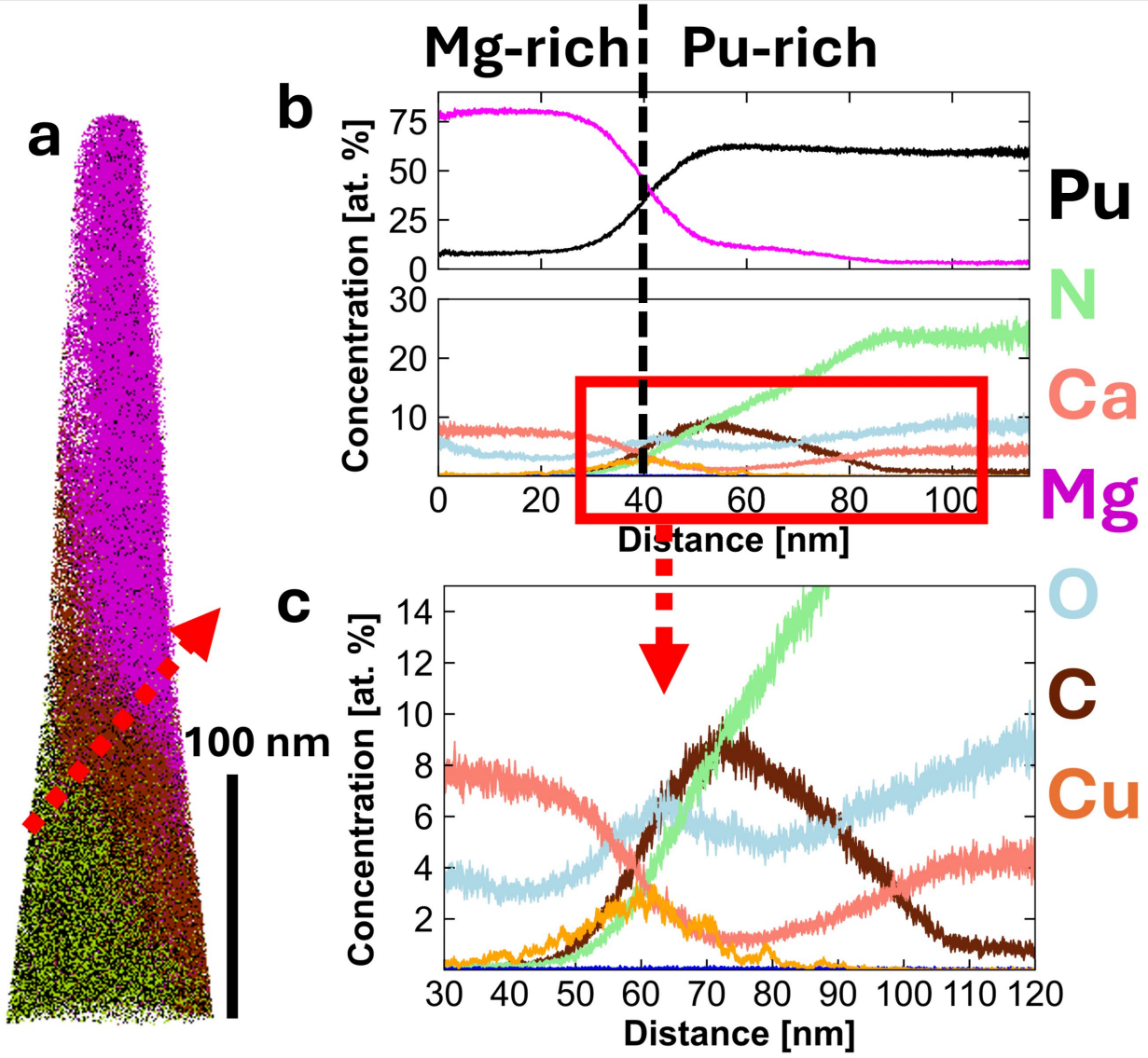

Figure 22. APT of a Mg/Pu Nitride interface. a) Ion map showing Mg (pink), C (brown), and Pu (Black). b) 1-Dimensional isoconcentration surface across the interface shown by the red dotted arrow on the ion map. c) Magnified region of interest showing across the interface.

The increase in Cu concentrations is not homogenous, however. The Cu is segregated into nanometer-sized clusters. **Figure 23a** shows the ion map with a dotted line that highlights the location of the Cu ions, magnified in **Figure 23b.** Nearest neighbor cluster algorithms then separated the ions into discrete clusters marked by different colors, **Figure 23c.** According to the sorting algorithm, discrete clusters are easily identified and not merely an artifact of random sorting. The chemical concentrations of the clusters were then analyzed and graphed as shown in **Figure 23d.** Inside of these nanoclusters, the mean concentrations of the clusters are primarily Cu with some outlying cluster reaching 100% Cu with trace amounts of Mg and Pu. The mechanism that would cause Cu clustering in this interface is not known. The origin of this low concentration of Cu in α-Pu is not clear, but it is probable that it was incorporated into the matrix during the hydrofluorination or bomb reduction processes. These figures reveal the utility of APT to help users understand the concentration of major and minor elements within a nanoscale volume of material.

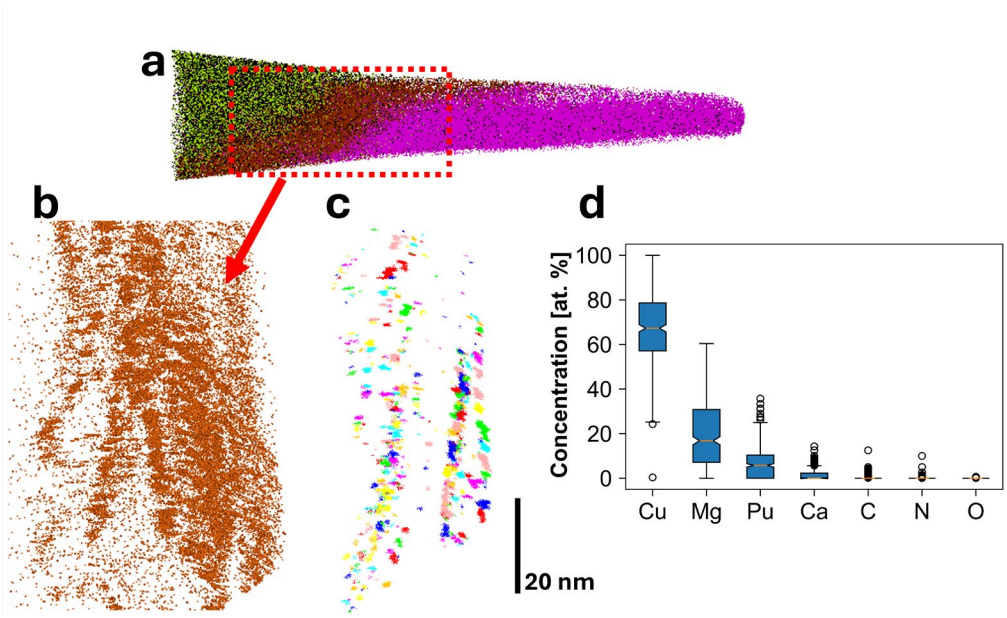

Figure 23. APT of a Mg/Pu Nitride interface. a) Ion map showing Mg (pink), C (brown), and Pu (Black). b) 1-Dimensional isoconcentration surface across the interface shown by the red dotted arrow on the ion map. c) Magnified region of interest showing across the interface.

5.0 Conclusions and Future Work

The work presented in this report documents the efforts of staff at PNNL to establish a Pu metallography capability at the RPL. Prior to FY23, PNNL was able to perform characterization of Pu metal, but staff were unable to cut and polish the samples on site. The capabilities and sample workflow were instituted over a relatively short period, FY23-24, and multiple characterization techniques were demonstrated using two forms of Pu metal. There are many more micrographs and analyses that were collected during this project. Some highlights of the findings of this report include:

- Development of an effective workflow for bulk to nano-scale characterization on α and δ-Pu at PNNL
- Identification of discrete Mg-bearing inclusions using SEM-EDS, S/TEM, and APT in as-bomb reduced α-Pu, which could be indicative of production method
- Nano-scale investigation of mechanically induced phase transformations in δ-Pu which could improve material science knowledge
- 3D spatially resolved analysis of alloying agents in δ-Pu (i.e., Ga) and impurities in α-Pu (i.e., Mg, Cu, N, Ca) which could help scientists and engineers understand the chemistry and composition of nanoscale inclusions and interfaces in bulk materials

The establishment of the Pu metallography capability at PNNL has created more opportunities for collaboration with other sites within the DOE Complex. By FY27, PNNL will expand these capabilities by installing them within an inert glove box, which will improve the quality and reproducibility of metallography on Pu metal. Currently, PNNL is investigating alternative polishing methods (i.e., vibratory, electro, and ion polishing) to reduce the damage caused by mechanical polishing and to enable surface sensitive characterization techniques such as EBSD.

6.0 References

1. Exner, H.E., *CHAPTER 10 - QUALITATIVE AND QUANTITATIVE SURFACE MICROSCOPY*, in *Physical Metallurgy (Fourth Edition)*, R.W. Cahn and P. Haasen†, Editors. 1996, North-Holland: Oxford. p. 943-1032.
2. Hecker, S.S. and M.F. Stevens, *Mechanical behavior of plutonium and its alloys.* Los Alamos Science, 2000. **26**: p. 336-355.
3. Wallace, P., W. Wien, and R. Goehner, *Mechanically-induced phase transformations in plutonium alloys.* Advances in x-ray analysis, 1988. **32**: p. 577-584.
4. Chang, Y., et al., *Ti and its alloys as examples of cryogenic focused ion beam milling of environmentally-sensitive materials.* Nature Communications, 2019. **10**(1): p. 942.

Pacific Northwest National Laboratory

902 Battelle Boulevard
P.O. Box 999
Richland, WA 99354

1-888-375-PNNL (7665)

www.pnnl.gov